Optically induced Faraday effect in a Λ configuration of spin-polarized cold cesium atoms

Jai Min Choi, Jang Myun Kim, Q-Han Park, and D. Cho*
Department of Physics, Korea University, Seoul 136-713, Korea
(Received 26 June 2006; published 26 January 2007)

Polarization rotation of weak probe light induced by circularly polarized strong coupling light in a Λ configuration is studied. We use spin-polarized cold cesium atoms trapped in a magneto-optical trap to remove complications from Zeeman distribution, Doppler broadening, and collisional decoherence. By using a very low probe intensity and short illumination period we work in a strictly linear regime. The probe and the coupling fields are optically phase locked to eliminate phase fluctuation and consequent atomic decoherence. Using this idealized situation we clarify the roles of optically induced Faraday rotation, circular dichroism, and electromagnetically induced transparency (EIT) in determining the final state of the probe light. In particular, we identify an experimental situation where the roles of atomic coherence and EIT are important.

DOI: 10.1103/PhysRevA.75.013815 PACS number(s): 42.50.Gy, 33.55.Ad, 42.25.Ja

I. INTRODUCTION

As an isotropic medium can be made either birefringent or optically active by the application of electric or magnetic fields, optical properties of an atomic vapor can be altered by illuminating the medium with polarized light. Chirality induced by optical pumping with circularly polarized light is one such example. While optical pumping relies on a dissipative process, properly polarized light can induce anisotropy of the medium through dispersive interaction. Circularly polarized light can induce a Zeeman-like ac Stark shift in an atom [1], and it can lead to an optically induced Faraday effect. In this case, the polarization of the weak probe beam is changed by the presence of a strong coupling beam via atomic nonlinear susceptibilities. Due to the low density of a vapor, it is necessary to use near resonant coupling and probe beams in a three-level lambda or ladder configuration. When the coupling light induces coherence among relevant atomic states in the three level system, the medium can exhibit the phenomenon of electromagnetically induced transparency (EIT) [2] for the probe light. This feature raises an intriguing possibility that a single coupling beam can render the medium both anisotropic and transparent.

Polarization rotation induced by a resonant two-photon process was first demonstrated for the $3S$-$3P$-$5S$ sodium transition in 1976 [3]. More recently, optically induced birefringence and Faraday rotation have been observed in the EIT framework for the $2S_1$-$2P_2$-$3S_1$ ladder configuration of metastable helium atoms [4]. Polarization control using the $5S_{1/2}$-$5P_{3/2}$-$7S_{1/2}$ configuration of rubidium atoms was also reported [5]. The S-P-S configuration has been used in an experiment that showed a laser-induced polarization change in ytterbium atoms [6], and in the theoretical study by Patnaik and Agarwal [7]. For these S-P-S ladder configurations driven by linear probe and circular coupling fields, only one circular component of the probe is affected by EIT. We theoretically studied the nS-nP-nD configuration to remedy the situation and also to clarify various effects contributing to the optically induced Faraday rotation (OFR) [8]. With the same motivation, OFR in a Λ configuration based on the rubidium $D2$ hyperfine transitions was recently studied using an atomic vapor [9].

Due to the near resonant situation, a probe beam inevitably suffers absorption as well as the polarization change. For the case of optically induced Faraday effect, asymmetric absorption of σ^+ and σ^- components leads to significant circular dichroism. On the other hand, near the two-photon resonance EIT plays an important role. Consequently, depending on the probe detuning there are complicated manifestations of circular dichroism, EIT, as well as OFR. Alkali metal atoms have hyperfine and Zeeman levels, and atoms in different Zeeman sublevels make different contributions to these effects. In addition, all of the experimental work carried out so far to study optically induced anisotropy used a vapor cell as an atomic medium. As the Doppler width is much larger than the frequency band where circular dichroism, EIT, or OFR is significant for a single atom, the Doppler averaging smears the underlying physics. For example, in the helium [4] and rubidium [5] experiments, although coherent polarization control using EIT was emphasized, it was not clear how atomic coherence or EIT manifested itself in the final results.

In this paper, we report on our experiment to clarify these issues in the optically induced Faraday effect using cesium atoms in a Λ configuration. The level scheme is basically the same as the one used in Ref. [9]. However, we use atoms trapped in a magneto-optical trap (MOT) to eliminate Doppler broadening. The trapped atoms are optically pumped to a single Zeeman sublevel to avoid complicated contributions from many sublevels. By using a very low probe intensity, we work in a strictly linear regime in a sense that the electric susceptibility of the medium for the probe field does not depend on the field itself. Less than 5% of atoms absorb probe photons. Finally, the coupling and probe light are optically phase locked to eliminate decoherence due to phase fluctuations.

II. EXPERIMENT

The level scheme used in the experiment is shown in Fig. 1. Cesium atoms are optically pumped to the $|6S_{1/2},F$

*Email address: cho@korea.ac.kr

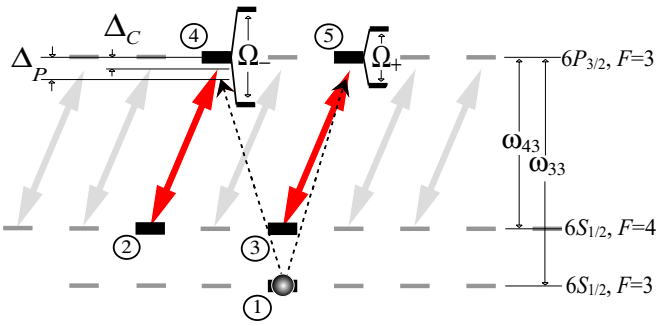

FIG. 1. (Color online) Level scheme of cesium atoms used in the experiment. Dotted lines are probe transitions and thick lines are coupling transitions. ①: $|6S_{1/2},F=3,m_F=0\rangle$; ②: $|6S_{1/2},F=4,m_F=-2\rangle$; ③: $|6S_{1/2},F=4,m_F=0\rangle$; ④: $|6P_{3/2},F=3,m_F=-1\rangle$; ⑤: $|6P_{3/2},F=3,m_F=+1\rangle$.

$=3,m_F=0\rangle$ state. The linearly polarized probe and the circularly polarized coupling fields are tuned to the $6S_{1/2}$, $F=3\rightarrow 6P_{3/2}$, $F=3$ and the $6S_{1/2}$, $F=4\rightarrow 6P_{3/2}$, $F=3$ transitions, respectively. ω_{33} and ω_{43} are the resonance frequencies of the corresponding $D2$ transitions. Δ_P and Δ_C are the detunings of the probe and the coupling fields from ω_{33} and ω_{43}, respectively. The ratio of the Clebsch-Gordan coefficients for the ③ to ⑤ and ② to ④ coupling transitions is $\sqrt{2/5}$ and the Autler-Townes splittings $\Omega_\pm$ for the $|6P_{3/2},F=3,m_F=\pm 1\rangle$ states have the same ratio. The electric susceptibilities for the σ^+ and σ^- components of the probe field become different and this induces chirality of the medium. In addition, the Λ configurations completed by the ①-④-② and the ①-⑤-③ transitions give rise to the EIT at the two-photon resonance.

A schematic diagram for the OFR apparatus is shown in Fig. 2. An extended cavity diode laser locked to the $6S_{1/2}$, $F=4\rightarrow 6P_{3/2}$, $F=3$ transition serves as a master laser. A 120-mW slave laser injection-locked to the master laser provides the coupling beam. Another extended cavity diode laser, optically phase-locked to the master laser with a 9.2-GHz frequency offset, provides the probe beam. The coupling beam is turned on and off by a mechanical shutter and it is mode matched to the atomic cloud with a diameter of 4 mm. Probe beam is switched with an acousto-optic modulator and it is transferred to the atomic cloud via an optical fiber. The probe beam diameter at the MOT center is 0.5 mm so that it is well covered by the coupling beam. The angle between the counterpropagating coupling and the probe beams is less than 10 mrad. It is exaggerated in Fig. 2. The relative size and the alignment of the beams are important to minimize inhomogeneous broadening. There are polarizing optics (not shown in the figure) that produce clean circular and linear polarizations for the coupling and probe beams just before the MOT chamber. The polarimeter placed further downstream measures the Stokes parameters of the transmitted probe beam. The coupling beam power is 6 orders of magnitude larger than the probe power, and its reflection off the fiber tip constitutes a large background. A solid etalon with 12.4-GHz free spectral range is inserted to block the reflected beam.

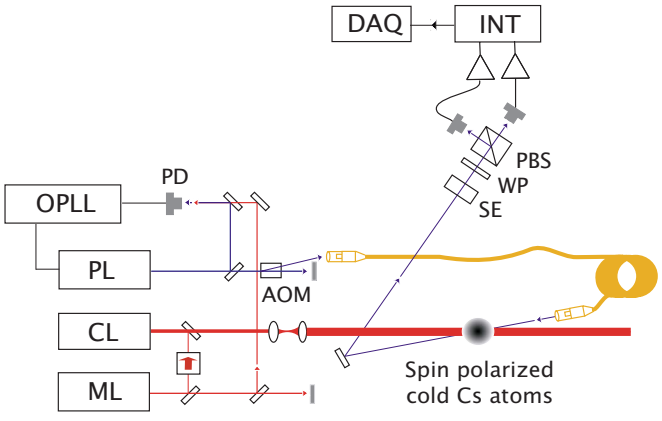

FIG. 2. (Color online) Schematic diagram for the optical Faraday rotation apparatus. ML: master laser; CL: coupling laser; PL: probe laser; OPLL: optical phase lock loop; PD: fast photodiode; AOM: acousto-optic modulator; SE: solid etalon; WP: waveplate, PBS: polarizing beam splitter; INT: gated integrators; DAQ: data acquisition system.

Each measurement cycle begins with a 150-ms MOT loading period which collects 3×10^8 atoms. At the end of the MOT loading, the repumping beam and the anti-Helmholtz coils are turned off and a single coil is turned on to define a quantization axis along the coupling and probe field propagation. The frequency of the trapping beam is then changed to the $6S_{1/2}$, $F=4\rightarrow 6P_{3/2}$, $F=4$ transition and a linearly polarized Zeeman pump beam tuned to the $6S_{1/2}$, $F=3\rightarrow 6P_{1/2}$, $F=3$ transition is turned on for 2 ms. This completes the optical pumping cycle and more than 50% of atoms are in the $|6S_{1/2},F=3,m_F=0\rangle$ state. Remaining atoms are more or less uniformly distributed among other Zeeman sublevels [10]. The single coil is turned off and after waiting for 2 ms for the transient B field to decay, the coupling and the probe beams are turned on. Signal from the polarimeter is integrated for 400 μs and stored. This cycle is repeated 10 times and the frequency offset from a synthesizer is increased by 500 kHz for the next probe frequency.

III. RESULTS AND DISCUSSION

We measure the parallel, perpendicular, +45°, −45°, σ^+, and σ^- components of the transmitted probe beam for the polarization analysis. Figure 3(a) shows the σ^+ and σ^- components versus Δ_P when $\Delta_C=0$. The vertical axis is normalized to half of the total transmitted power without atoms, and the horizontal axis to the decay rate of the $6P_{3/2}$ state, $\Gamma_P=2\pi\times 5.2$ MHz. Figure 3(b) shows the +45° and −45° components. For these measurements the coupling and the probe intensities are 70 mW/cm^2 and 0.6 μW/cm^2, respectively. The optical depth of the atomic cloud inferred from the data is 5.1. The solid lines represent theoretical curves calculated by solving master equations [8]. Except for some of the sharp features the data points agree with the theory reasonably well. However, incomplete optical pumping and residual inhomogeneity of the coupling intensity over the probe beam profile lead to an inhomogeneous broadening. In order to account for the broadening phenomenologically, we have to use $2.5\Gamma_P$ as an effective decay rate of the $6P_{3/2}$ state

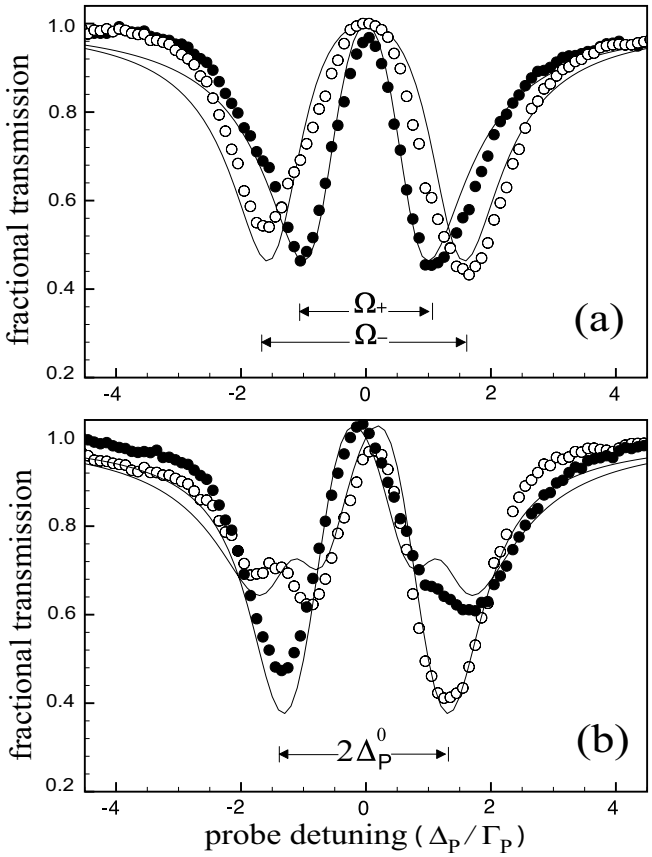

FIG. 3. (a) Normalized transmitted probe beam powers for the σ^+ (●) and σ^- (○) components and (b) for the +45° (●) and −45° (○) components versus Δ_P/Γ_P when $\Delta_C=0$. Solid lines represent theoretical curves for corresponding components.

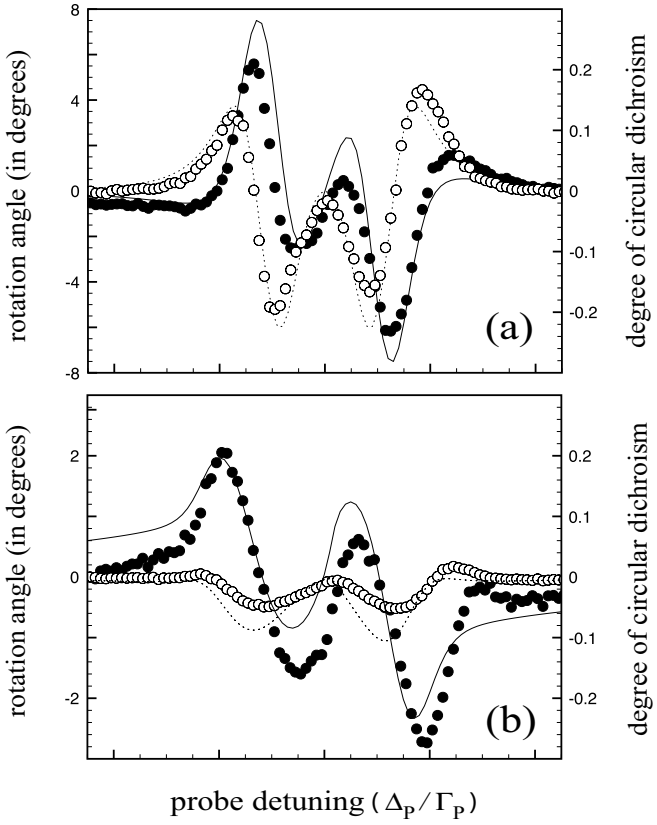

FIG. 4. Rotation angle ψ (●) and degree of circular dichroism $\sin 2\chi$ (○) (a) with and (b) without the optical pumping. Dotted and solid lines represent theoretical curves.

in the master equation. Each of the σ^+ and σ^- components in Fig. 3(a) shows a spectrum with an Autler-Townes splitting. We note that there is almost 100% transmission at $\Delta_P=0$ due to EIT. The ratio of the splittings Ω_+/Ω_- in Fig. 3(a) is 0.60, which agrees with the theoretical value of $\sqrt{2/5}$. The difference in the splittings leads to a frequency offset of 1.5 MHz between the pairs of σ^+ and σ^- transmission minima. The frequency offset is analogous to a differential Zeeman shift in the Faraday effect [12]. Unlike the regular Faraday effect, which produces a splitting of σ^+ and σ^- components centered at $\Delta_P=0$, there are two pairs of split dips centered around $\pm\Delta_P^0$ where $\Delta_P^0=(\Omega_+ + \Omega_-)/2$.

From the measured polarization components we extract ψ and $\sin 2\chi$ [11], where ψ is a rotation angle of the major axis of an elliptic polarization and $\sin 2\chi$ is a degree of circular dichroism,

$$\sin 2\chi = \frac{P_{\sigma+} - P_{\sigma-}}{P_{\sigma+} + P_{\sigma-}}.$$

$P_{\sigma\pm}$ are the transmitted powers of the $\sigma^\pm$ components. Figure 4(a) shows ψ and $\sin 2\chi$ with the optical pumping and Fig. 4(b) without it. In Fig. 4(a) ψ is largest near $\pm\Delta_P^0$, where the circular dichroism vanishes [see Fig. 3(a)] and the probe polarization is linear. We note from Fig. 3(a), however, that both circular components are absorbed by 45% at $\pm\Delta_P^0$. Near $\Delta_P=0$, where absorption is small due to EIT, the real part of susceptibility is also small due to the Kramers-Kronig relations and there is no significant polarization change. This is a general feature of optically induced birefringence or Faraday rotation: The region of large transmission is disjoint from that of large polarization change. The curves for ψ and $\sin 2\chi$ without spin polarization in Fig. 4(b) are broadened with much reduced features. The maximum rotation angle is only one third of that with the optical pumping. Atoms in different Zeeman sublevels produce overlapping contributions with frequency offset from each other. The experimental data and theory curves show poor agreement because of the uncertainties in Zeeman population produced by the MOT and residual ambient B field.

Our results in Fig. 3 and Fig. 4(a) can be compared with a similar measurement using a room-temperature rubidium vapor cell [9]. Unlike the clearly resolved double dips in Fig. 3(a), transmission spectra of the σ^+ and σ^- components through the vapor cell have single peaks at $\Delta_P=0$ due to EIT, albeit with different widths. Doppler broadening, averaging over Zeeman distribution, and decoherence from atomic collisions results in a smooth dispersion shape without the distinctive features shown in Fig. 4(a).

In Fig. 5 we show ψ for the spin polarized sample with right and left circularly polarized coupling beams. Helicity of the coupling beam plays the role of the direction of an effective B field, and the sign of ψ is reversed under the polariza-

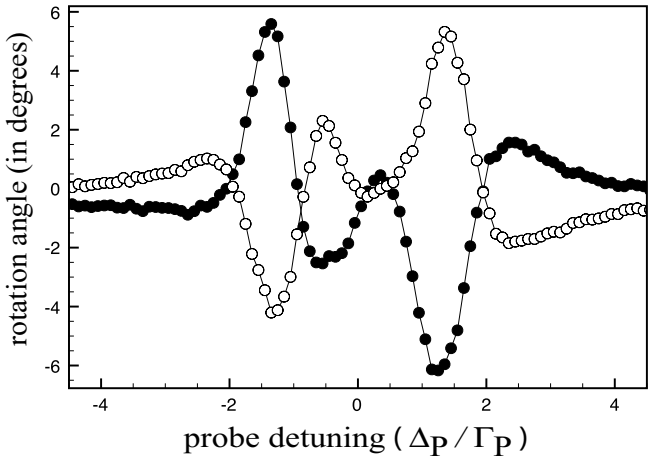

FIG. 5. Change in the sign of the rotational angle ψ under the polarization reversal of the coupling field: When the coupling polarization is σ^+ (●) and when it is σ^- (○). The solid lines are to guide the eye.

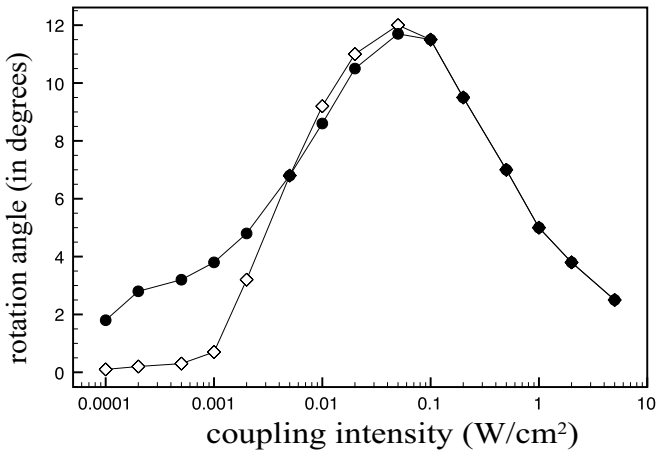

FIG. 6. Calculated maximum rotation angle $\psi_{\max}$ for spin-polarized cold cesium atoms at $\Delta_P=\Delta_P^0$ versus coupling intensity when the atomic coherence is considered (●) and when it is not considered (◇).

tion reversal. Figure 6 shows the theoretical predictions for $\psi_{\max}$ at $\Delta_P=\Delta_P^0$ for the spin-polarized cold sample as the coupling intensity is changed over five orders of magnitude. The curve for the filled circles represents results from solving master equations for the Λ configuration taking into account atomic coherence and EIT. The curve for the diamonds represents results without considering atomic coherence. The coupling beam produces Autler-Townes splittings and the electric susceptibility χ_e for the probe field is calculated by summing χ_e from individual transitions from the ground state to each of the split states, which are assumed to be independent. Both curves peak at the coupling intensity of 50 mW/cm^2. We note that above 5 mW/cm^2 the two curves are almost identical and the probe polarization change can be explained by a differential ac Stark shift without invoking atomic coherence. It is only when the coupling intensity is low enough for the width of the EIT peak to be much smaller than the natural linewidth that the coherence plays a major role in the polarization control. The situation in this low-intensity limit is analogous to an enhancement of optical nonlinearity through atomic coherence [13]. We could not carry out measurement of optically induced Faraday effect at such a low coupling intensity because uncontrolled ambient magnetic field and residual phase fluctuation of the laser fields limited linewidth of EIT peaks.

IV. SUMMARY

We have studied an optically induced Faraday effect in an experimental situation where atomic motion and spin state are tightly controlled. We identify frequency regions where OFR, circular dichroism, and EIT become important in determining the polarization state of the probe field. We find that in order to observe coherence effect one has to use a coupling intensity far below the saturation intensity.

ACKNOWLEDGMENTS

This work was supported by the Korea Science and Engineering Foundation (R01-2005-10477) and by the Seoul R&BD program. We thank T. H. Yoon for help with the optical phase locking.

[1] C. Cohen-Tannoudji and J. Dupont-Roc, Phys. Rev. A **5**, 968 (1972); D. Cho, J. Korean Phys. Soc. **30**, 373 (1997).
[2] K.-J. Boller, A. Imamoğlu, and S. E. Harris, Phys. Rev. Lett. **66**, 2593 (1991).
[3] P. F. Liao and G. C. Bjorklund, Phys. Rev. Lett. **36**, 584 (1976).
[4] F. S. Pavone, G. Bianchini, F. S. Cataliotti, T. W. Haensch, and M. Inguscio, Opt. Lett. **22**, 736 (1997).
[5] S. Wielandy and A. L. Gaeta, Phys. Rev. Lett. **81**, 3359 (1998).
[6] T. H. Yoon, C. Y. Park, and S. J. Park, Phys. Rev. A **70**, 061803(R) (2004).
[7] A. K. Patnaik and G. S. Agarwal, Opt. Commun. **179**, 97 (2000); A. K. Patnaik and G. S. Agarwal, *ibid.* **199**, 127 (2001).
[8] D. Cho, J. M. Choi, J. M. Kim, and Q. Han Park, Phys. Rev. A **72**, 023821 (2005).
[9] B. Wang, S. Li, J. Ma, H. Wang, K. C. Peng, and M. Xiao, Phys. Rev. A **73**, 051801(R) (2006).
[10] J. M. Choi, J. M. Kim, J. H. Lee, Q. Han Park, and D. Cho, Phys. Rev. A **71**, 043409 (2005).
[11] Born and Wolf, *Principles of Optics*, 6th ed. (Pergamon, New York, 1980).
[12] We may define the effective B field by equating the frequency offset $(\Omega_- - \Omega_+)/2$ to $2g_F\mu_B B$, where g_F is the Landé g factor and μ_B is the Bohr magneton. g_F for the $6P_{3/2}, F=3$ state, however, is 0 and it is ambiguous in this case.
[13] S. E. Harris, J. E. Field, and A. Imamoğlu, Phys. Rev. Lett. **64**, 1107 (1990).